Development of injection molding simulation algorithms that take into account segregation

Ferenc Szabó [a], András Suplicz [a,*], József Gábor Kovács [a,b]

[a] Department of Polymer Engineering, Faculty of Mechanical Engineering, Budapest University of Technology and Economics, Műegyetem rkp. 3., H-1111 Budapest, Hungary
[b] MTA-BME Lendület Lightweight Polymer Composites Research Group, Műegyetem rkp. 3., H-1111 Budapest, Hungary

ARTICLE INFO

ABSTRACT

The quality of injection molded products is influenced by several factors: the geometry of the product, the polymer used, the mold, the technological parameters of processing and the injection molding machine itself. For this reason, modelling the process by computer is justified and widely used in the industry. Modelling, however, is complicated by the complex flow dynamic and thermal processes during injection molding, and the changes in the material structure of the polymer. Various fillers are used to modify the properties of the polymer, which is an additional challenge for simulation. Processing can cause variation in local filler content in the polymer, which influences several properties of the polymer, but available injection molding software cannot handle the distribution of fillers during the molding process yet, reducing the accuracy of simulations. In this project, we investigated the behavior of polypropylene filled with glass beads during injection molding. For the tests, we prepared mixtures of various filler contents and different bead sizes by extrusion. We also measured the effect of different injection molding parameters, and we examined the segregation of fillers. We modelled segregation numerically with Autodesk Moldflow, and calculated segregation from the results by discrete element modelling.
© 2021 The Authors. Published by Elsevier B.V. This is an open access article under the CC BY-NC-ND license (http://creativecommons.org/licenses/by-nc-nd/4.0/).

1. Introduction

In the past decades, the plastic industry has become one of the largest industries. In 2018, 359 million tons of polymer products were produced. As a result, the plastic industry is the 7th largest industry in Europe [1]. Nowadays injection molding is one of the most widely used processing technologies for polymers, accounting for 30% (by mass) of all polymer products. The dynamic development of the industry, the complicated geometry of injection molded products and the complex changes in material structure during injection molding necessitate its computer simulation. Injection molding simulation helps optimize manufacturing, leading to a considerable saving in time and cost, and improvement in quality, but the accuracy of simulation is greatly influenced by the accuracy of the models used [2].

If the probability of finding a particle in certain regions of a mixture (e.g. particle concentration) differs from the probability of finding a particle in the whole system, it is called segregation.

In the case of polymers containing fillers, the main issue is local filler concentration, in which the differences can cause visual problems [3,4]. In the case of reinforced polymers, the orientation of the reinforcement also plays a very important role. There are several methods to examine orientation [5,6], and its simulation is an intensively researched area [7,8].

Hegler and Menning [9] investigated the difference between the segregation of fiber reinforcement and spherical fillers. While the segregation of reinforcing fibers along the flow path was negligible during injection molding, the segregation of glass beads increased considerably at the end of the flow path compared to the nominal concentration. Kovács [10] examined segregation and its effect on shrinkage using PA6 as matrix, with glass beads of different sizes. His results highlight that glass beads of different sizes cause a different degree of segregation, and the effect of segregation on shrinkage cannot be neglected. Colón Quintana et al. [11] examined segregation during extrusion and injection molding with the use of CT images. Several methods have been suggested for the continuum modelling of particles in a flow [12–15]. Nowadays, as computers are more powerful, the discrete element modelling of the behavior of particles is playing a more and more important role [16–18]. With the use of coupled FEM-DEM analysis, the interaction of flowing liquids and particles can be modelled [19–21]. Polymer composite processing technologies develop quickly. By 2020, 3D printing composites with carbon or glass fiber is also possible [22–24]. 3D printing is used combined with injection molding as well and the fact that even processing foam with it is possible proves how versatile injection molding is [25,26]. DEM modelling is already used in the field of composites, and several studies focusing on it have been published [27–30].

---

* Corresponding author.
E-mail addresses: szabof@pt.bme.hu (F. Szabó), suplicz@pt.bme.hu (A. Suplicz), kovacs@pt.bme.hu (J.G. Kovács).

The segregation of the fillers can cause inhomogeneities in the local properties of injection molded products, which can decrease the accuracy of simulation results. So far no method has been developed to handle the modelling of segregation in injection molding, therefore our goal is to develop a new simulation method to model segregation during injection molding with the use of injection molding simulation and discrete element modelling.

2. Materials and methods

2.1. Materials used

The tests were performed on flat polypropylene specimens filled with glass beads. The nominal dimensions of the specimen were 80 mm × 80 mm × 2 mm, as this geometry is particularly suitable for the examination of segregation along the flow path (Fig. 1).

We manufactured nine polymer–filler mixtures from a PP matrix (MOL Tipplen H145 F), using three filler concentrations and Cerablast glass beads of three different size ranges (Table 1).

Before compounding, we divided the glass beads into three size ranges using a BA 200 N sieve shaker. Then we prepared compounds on an LTE 25–30/C extruder. During compounding, rotational speed was 25 1/min and melt temperature was 210 °C.

2.2. Measurement methods

The specimens were injection molded on an Arburg Allrounder 370S 700–290 injection molding machine (for process parameters, see Table 2). We examined the effect of injection rate on segregation using three injection rates (5 cm³/s, 20 cm³/s and 80 cm³/s) with all mixtures. To examine segregation along the flow path, we cut the specimens into four equal parts (see Fig. 1). Then we determined the filler content of the parts by matrix burnoff.

In order to determine the actual filler content, we placed the samples in ceramic cups with known weights. After that, the samples in the ceramic cups were placed in a Denkal 6B type calcination chamber. The samples were kept at 600 °C for 4 h based on the ISO 3451-1 standard, until the matrix material burnt completely. After determining the weight of the residual material, we calculated the glass bead content of the samples with the following equation:

$$\varphi = \frac{m_{ash} - m_{cup}}{m_{sample+cup} - m_{cup}} \cdot 100 [\%] \tag{1}$$

where m_{ash} is the residual weight after calcination, m_{cup} is the weight of the ceramic cups, while $m_{sample+cup}$ is the weight of the sample to be measured and the ceramic cup together.

2.3. Injection molding simulation

We performed simulations with the Autodesk Moldflow Insight 2018 simulation software. The finite element mesh of the simulation
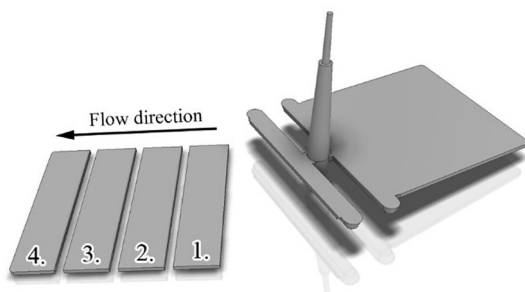

Fig. 1. Flat specimen for the tests.

Table 1
The glass bead content of the specimens.

Concentration [wt%]	Diameter range [μm]		
10	75–125	125–250	>250
25	75–125	125–250	>250
40	75–125	125–250	>250

Table 2
Injection molding parameters.

Parameter	Value
Mold temperature	30 °C
Melt temperature	230 °C
Injection rate	5 cm³/s, 20 cm³/s, 80 cm³/s
Holding pressure	500 bar
Holding time	5 s
Residual cooling time	15 s

models was made up of tetrahedron elements of 5 mm edge length in the flow direction. To calculate the thickness of the frozen layer accurately, we set minimal element number along the thickness to 20, therefore the typical average element size along the thickness was 0.1 mm. The model created this way consisted of 377 thousand elements. We only modelled filling as this is the phase when a considerable amount of polymer flows so this phase is expected to be dominant from the point of view of segregation. We set the parameters of simulation according to the parameters we used in the actual injection molding experiments. In the solution, the time steps are also influenced by the volume that can be newly filled, and also, it is possible to limit the maximum of the volume filled in a time step. We set the latter parameter to 4%, therefore the maximum of the time steps are 0.1 s with the slowest flow rate, 0.05 s when the fill rate is 20 cm³/s, and 0.0125 s with the highest flow rate. To define the material models, we performed pvT, DSC, thermal conductivity and viscosity tests.

The pvT data of pure PP were determined with a PistonDie dilatometer. We determined the pvT data of the various glass bead-PP compounds with the use of the pvT data of unfilled PP and the rule of mixtures. After the data points of the pvT curves for the filled material were calculated, we fitted the Tait equation, and entered its parameters in the database.

We determined the specific heat by performing a DSC test with a TA Q2000 instrument between 0 °C and 300 °C, with a cooling rate of 5 °C/min.

The thermal conductivity coefficient was measured with a special, asymmetric hot plate apparatus at 55 °C.

We determined the viscosity curves with a capillary rheometer (Ceast SR 50) and a rotational rheometer (Anton-Paar Physica MCR 301) using the shear rate range characteristic to injection molding. Rotational rheometer tests were carried out in a plate-plate layout, with a gap size of 1 mm at three different temperatures (150 °C, 190 °C and 240 °C).

2.4. Simulation of segregation

The basic model of the segregation of particles in injection molded products is depicted in Fig. 2. The base of the method is the investigation of the flow of molten polymer during the high-temperature injection molding process and its frozen layer fraction developing next to the wall of the mold. Our theory is that the flow of the polymer melt can tear out the semi-embedded particles and return them into the flow. The model is based on the fact that the concentration of the filler along the melt flow is dependent on how much the flow forces tear
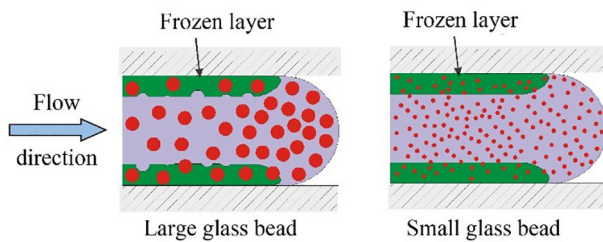
Fig. 2. The basic model of segregation.

the particles from the frozen layer. Accordingly, the frozen layer should be investigated as a function of time during the injection molding process (which injection molding simulations are capable of) and so should the movement of the particles returning to the flow and their interaction with their environment (which injection molding simulations are not capable of). The extent of segregation will most probably be influenced by the thickness of the frozen layer, since during its growth, particles from more and more volume can be torn out. Another important parameter is the nominal size of the filler, since smaller size fillers most probably embed more into the continuously growing frozen layer next to the wall of the mold. During the process, the melt flow rate could be a significant impact factor in many aspects. An increase in flow rate increases the amount of heat transported by the material as well as the shear-induced heat due to the high viscosity, which both have an effect on the thickness of the frozen layer. Additionally, an increasing flow rate most probably increases the flow forces affecting the embedded particles.

We used a mechanical model and performed CFD simulations to investigate under what conditions the flow forces can tear the particles out of the frozen layer. Fig. 3 shows the mechanical model of tearing a particle out. Not only flow and adhesion forces but also internal pressure and vacuum act on the particles at the moment they are torn out, since the high-viscosity polymer melt must flow back into its original position. In boundary conditions, the momentum caused by the flow forces is higher than the effects of the other components, thus it rotates the sphere around point "A" and returns it to the melt flow. The extent of embedding affects all force components, thus we investigated the extent momentum acted on 70 μm and 250 μm size, ½, ¼ and 1/8 embedded spheres. During the calculation, the adhesion forces were neglected, since based on our previous investigations, the adhesion between the glass and the PP is low. We calculated the flow forces acting on the material with the Autodesk CFD 2018 software by applying a deformation and temperature-dependent viscosity model. The calculations were done for both the lowest and highest typical flow rates. Fig. 4 shows the momentum acting on the fillers. As can be seen, at higher shear rates, the flow forces significantly increase, thus the melt flow most probably tears
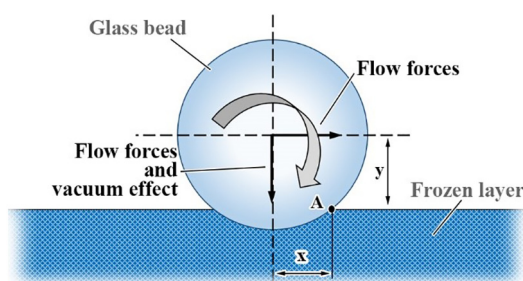

Fig. 3. The mechanical model of the phenomenon.

out and returns to the flow particles with more than half the surface area sticking out of the frozen layer. At lower flow rates, due to the decrease in flow forces, the particles are more stable, thus they stay in the frozen layer even if less of the particle is embedded. Since high shear rates are characteristic of injection molding, the boundary condition for tearing particles out should be adjusted accordingly.

We performed coupled FEM-DEM simulation to model segregation in the polymer. For discrete element modelling, we connected the data calculated by Moldflow with the discrete element modelling panel written in Matlab using a plug-in module (solver API). Due to the geometry of the part, we built a 2.5 dimension model; we assumed that along the whole width of the part, the distribution of the speed of the molten material is the same as in the middle. We assumed that the calculated flow speed distributions do not change between the time steps, and used linear interpolation to determine the characteristic speeds in the space between the nodes. The effect of the runner on segregation was neglected; the particles entered the simulated material flow at the gate. Their size distribution was monodisperse and their diameter was 75 μm, 125 μm and 250 μm. The particles were created within the walls of the gate randomly, with uniform dispersion, at a distance of at least their radius from each other and the surface of the gate. The dimension of the applied film gate is 80 mm × 1.2 mm × 1 mm. The cross-section change of the gate during the process was neglected due to the heat transferred by the fresh polymer. During the calculations, the flow force acting on the particles was taken into account with the drag force model. Due to the high viscosity of the polymer, the particles are accelerated in the direction of the flow by a force considerably larger than their weight. Accordingly, during solving the DEM problem, only very small time steps can be used, which highly increases calculation time, thus the flow forces were determined so that they should accelerate the particle to the flow rate in one time-step. As a result, if a glass bead gets embedded into the frozen polymer layer in a depth of at least its radius, it stops moving; the material flow cannot tear it out. If the depth of embedding is less than the radius of the particle, the flow removes and takes the particle away from the frozen layer. The collisions of the particles with each other and with the wall were modelled with the linear spring contact model. We determined spring stiffness taking into account particle size and characteristic maximal flow speed so that the maximal overlap between colliding particles does not exceed 5%. We used Eq. (2) to calculate the maximal time step from the mass (m) of particles and spring stiffness (k) [31].

$$\Delta t_{crit} = 0.3 \cdot \sqrt{\frac{m}{k}} \qquad (2)$$

Table 3 contains the spring stiffnesses and time steps.

3. Results

The difference in glass bead content measured at the beginning and at the end of the flow path as a function of injection rate is shown in Fig. 5. It can be seen that in the case of 75 μm and 125 μm nominal size glass beads, segregation is higher at a low injection rate (5 cm³/s), than at higher injection rates. At the same time, there were no significant differences between the injection rates of 20 cm³/s and 80 cm³/s. In the case of 250 μm glass beads, there was a decreasing tendency in filler content differences at higher injection rates, but in this case, there was a significant change between 5 cm³/s and 20 cm³/s. Subsequently, the process of segregation is defined mostly by the geometry of the filler, its size and the flow conditions of the given mold.

We investigated filler dispersion at a given filler content and at a flow rate of 20 cm³/s (Fig. 6). The diagrams show that at low filler concentrations, segregation is negligible with 75 μm and 125 μm size glass
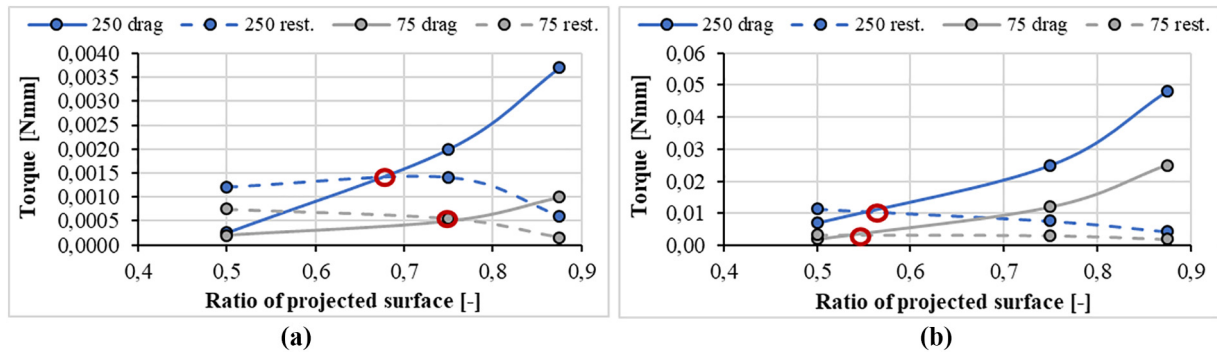
Fig. 4. Momentums acting on the particles at an injection rate of 5 cm^3/s (a) and 80 cm^3/s (b).

Table 3
The spring stiffnesses and time steps applied.

Particle diameter [μm]	80 cm^3/s		20 cm^3/s		5 cm^3/s	
	k [N/m]	Δt_{crit} [μs]	k [N/m]	Δt_{crit} [μs]	k [N/m]	Δt_{crit} [μs]
75	120	0.656	11	2.16	1.2	6.56
125	200	1.1	18	3.65	2	10.9
250	400	2.19	35	7.4	4	21.9

beads. When 250 μm size glass beads were used, the difference in concentration between the beginning and the end of the flow path was 3–4%. With increased filler content, this difference increased. In the

case of small particles, this increase was only a few percent, but with 250 μm glass beads, the increase was much more significant. At 25 m% and 40 m% glass bead contents, the difference was 8.8 m% and 10.9 m %, respectively.

Fig. 7 shows the temperature distribution along the cross-section at various injection rates determined by injection molding simulation. By the end of the filling phase, the different flow rates caused a highly different temperature profile along the cross-section of the product. The parts below 130 °C are already in the solid state, while the hotter parts are still in the molten state.

The frozen layer is the thickest in the middle of the product, since the hot polymer melt entering the flow slows the freezing of the material. On the contrary, at the end of the flow path, the thinner frozen layer is caused by the shorter cooling time. The effect of significant differences can also be seen in the data.
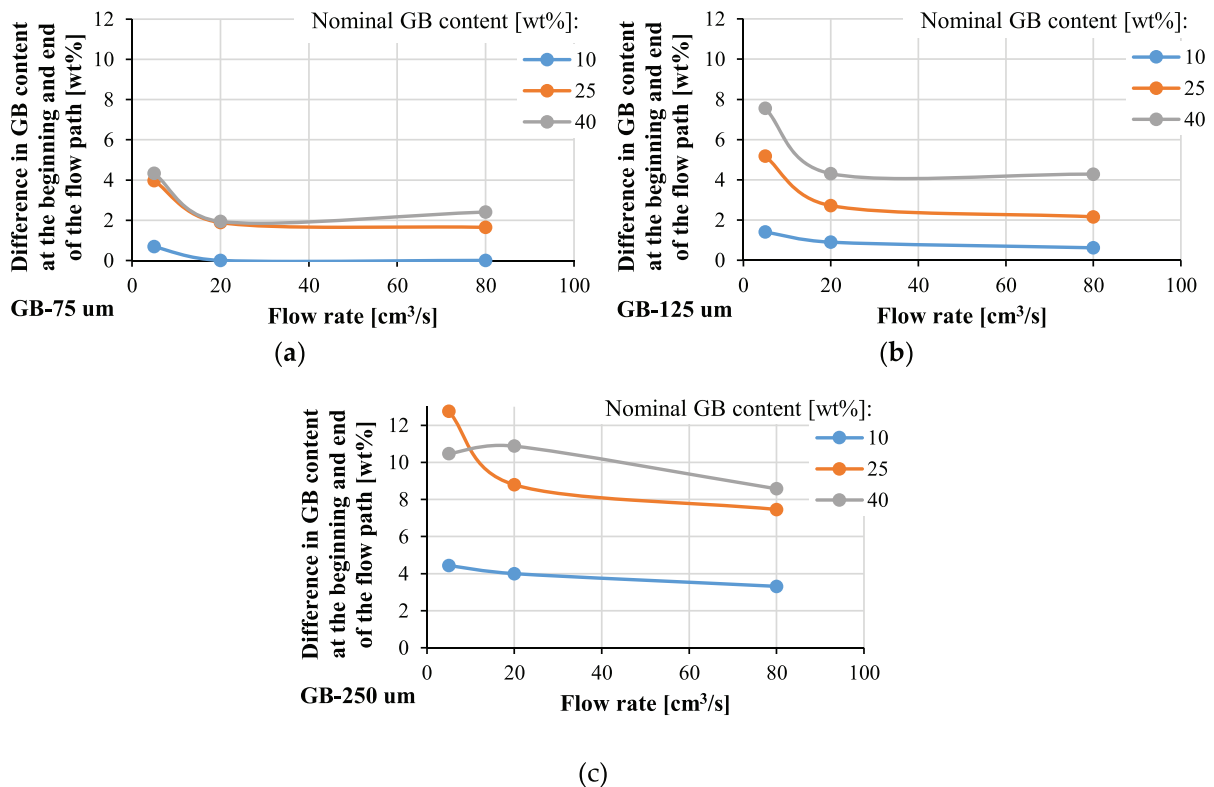

Fig. 5. Difference in glass bead content at the beginning and at the end of the flow path as a function of injection rate with the use of glass beads (GB) of different diameters.
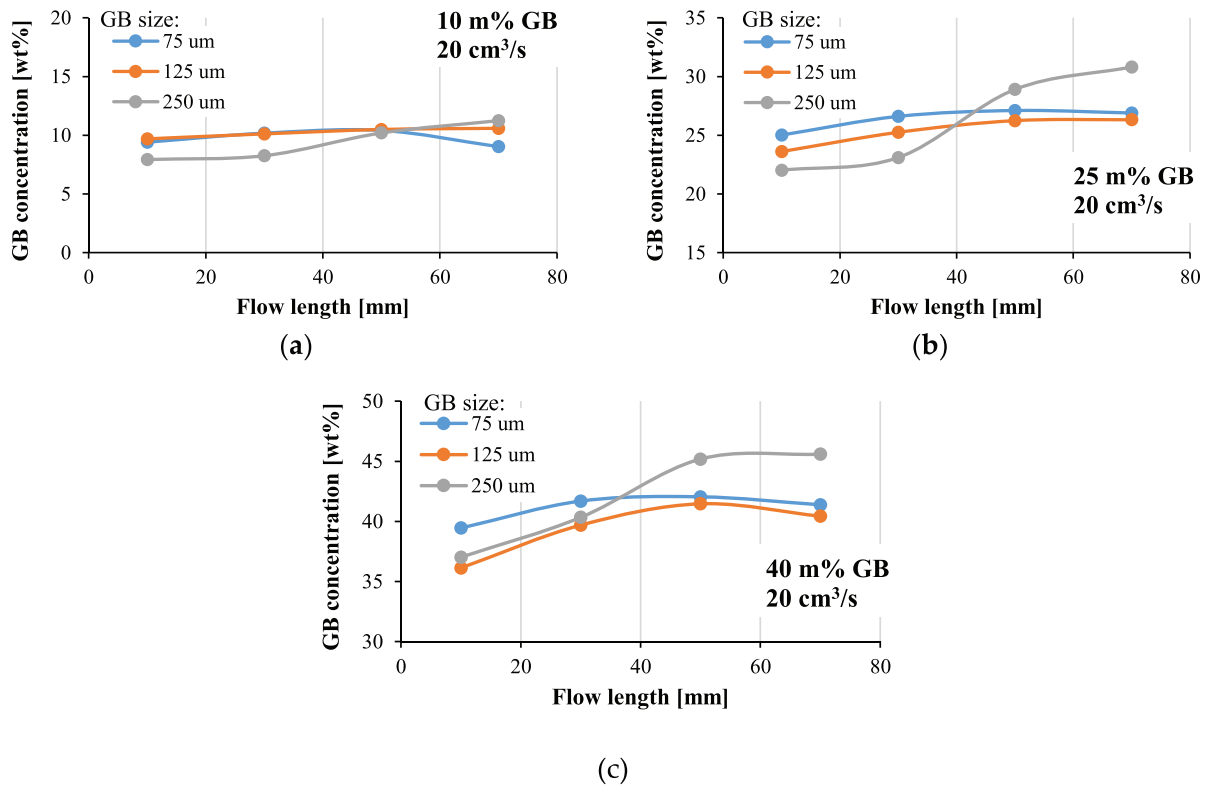
Fig. 6. Glass bead concentration along the flow length as a function of injection rate and nominal filler content.

In this article, we only show the evaluation of calculations along the flow path. Fig. 8 shows the calculated and measured data at an injection molding rate of 20 cm³/s in the case of the three investigated glass bead sizes and contents. The calculated results approximate actual conditions well: as particle size increases, segregation increases too. The tendency is also similar in the case of increasing filler content.

As can be seen, the algorithm overestimates filler content at the beginning of the flow path and underestimates it at the end of the flow path in the case of 75 μm. This can be explained by the decrease in the cross-section of the gate, which is not taken into account by the algorithm. Accordingly, particle concentration increases near the walls where the melt is cooling and so the flow rate is lower, and so the particles only travel to the beginning of the flow path. In the case of larger

filler size, this neglection has lower significance, since the larger particles cannot approach these slow parts. Fig. 9 shows the calculated and measured filler content at the flow rate of 5 cm³/s and the nominal filler content of 40 m%. At the end of the flow path, the calculated results overestimate real filler content, and there were also high differences in the middle of the flow length. This can be explained by the tear-out criteria applied in the calculations, which determine tearing out below 50% embedment. Based on the CFD calculations, this is not accurate enough at low flow rates, thus the filler content of the frozen layer decreases and the torn-out particles increase the filler concentration at the end of the flow path.

The difference between the measured and simulated results were characterized by the root mean square error (RMSE), determined by the following equation:

Fig. 7. The temperature distribution of the injection molded specimens at various flow rates.
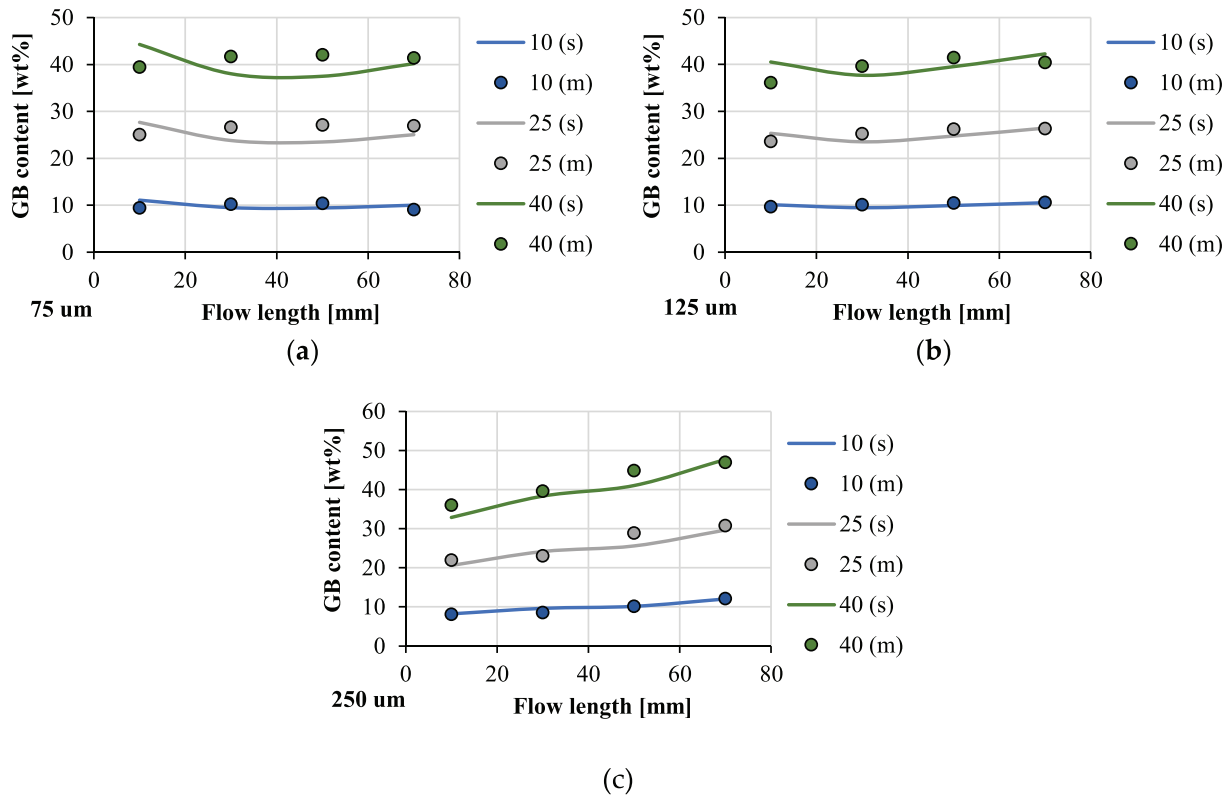
Fig. 8. Comparison of the measurement (m) and simulation (s) results with the use of glass beads of different sizes.
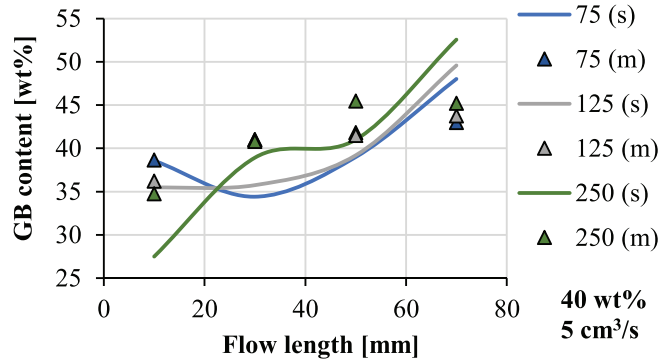

Fig. 9. Comparison of the measurement (m) and simulation (s) results with the use of different size glass beads (nominal filler concentration: 40 wt%, injection rate: 5 cm³/s).

$$RMSE = \sqrt{\frac{1}{n} \sum_{i=1}^{n} \left(m_{s,i} - m_{m,i} \right)^2} \qquad (3)$$

where m_s is the filler content obtained by simulation and m_m is the measured filler content. As injection rate increases and filler content decreases, the correspondence between the measured and simulated data increases. The results indicate that the method we developed is suitable for modelling filler segregation during injection molding. The accuracy of the method can be further improved by taking the neglected factors into account (Fig. 10).

The accuracy of the injection molding simulation algorithm can be improved to take into account filler concentration, as filler concentration influences the input data of the simulations. As filler concentration changes, the viscosity of the polymer material can change significantly. Present commercial software (for example Moldflow, Moldex3D) cannot handle this phenomenon. Through the API surface of Moldflow,
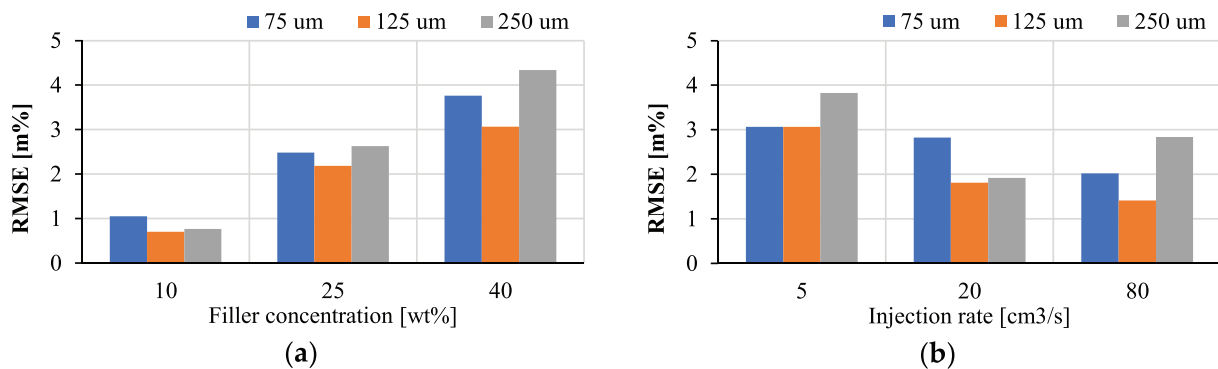

Fig. 10. RMSE values of the simulation results.

two-way communication can be allowed. In this way, the software will be able to handle filler concentration dependent viscosity models as we improve the applied plugin.

4. Conclusions

Our goal was to investigate and model segregation during injection molding. We examined segregation with injection molded flat specimens composed of a PP matrix and glass beads of different sizes and concentration. We also varied injection rate, and this way the thickness of the layer of frozen polymer. We found that segregation increases considerably above the particle size of 125 μm, it decreases with injection rate, and increases with particle concentration.

The filler concentration difference is over 12%, which significantly changes the viscosity and pvT properties of the material. If these effects are neglected, the accuracy of the simulation will decrease.

In our model, segregation during injection molding is caused by the partially embedded particles. Hence the differences in local filler concentration are determined by the thickness of the frozen layer and the amount of particles torn out. The CFD simulations show that a spherical particle can be torn out of the frozen layer if it is embedded less deep than its radius. We calculated the flow rate field during injection molding with Autodesk Moldflow Insight 2018. Discrete element problems were solved with MATLAB.

According to the results, the algorithm can describe the expected local glass bead concentration with high accuracy in the injection rate range of 20–80 cm^3/s. If the algorithm is improved, accuracy can also improve in the case of lower injection rates. The results indicate that the newly developed method is able to model segregation in injection molding, therefore it can improve injection molding simulation by eliminating inaccuracies caused by inhomogeneities.

Declaration of Competing Interest

The authors declare no conflict of interest.

References

[1] Plastics Europe: Plastics – The Facts 2019, an Analysis of European Plastics Production, Demand and Waste Data, https://www.plasticseurope.org/application/files/9715/7129/9584/FINAL_web_version_Plastics_the_facts2019_14102019.pdf 2019.

[2] Z. Huamin, Computer Modeling for Injection Molding: Simulation, Optimization, and Control, John Wiley & Sons, New Yersey, 2013.

[3] L. Zsíros, J.G. Kovács, Surface homogeneity of injection molded parts, Period. Polytech. Mech. Eng. 62 (4) (2018) 284–291, https://doi.org/10.3311/PPme.12128.

[4] D. Török, J.G. Kovács, Effects of injection molding screw tips on polymer mixing, Period. Polytech. Mech. Eng. 62 (3) (2018) 241–246, https://doi.org/10.3311/PPme.12183.

[5] X. Sun, et al., Measurement and quantitative analysis of fiber orientation distribution in long fiber reinforced part by injection molding, Polym. Test. 42 (2015) 168–174, https://doi.org/10.1016/j.polymertesting.2015.01.016.

[6] K. Albrecht, E. Baur, H.-J. Endres, R. Gente, N. Graupner, M. Koch, J. Müssig, Measuring fibre orientation in sisal fibre-reinforced, injection molded polypropylene – pros and cons of the experimental methods to validate injection molding simulation, Compos. A: Appl. Sci. Manuf. 95 (2017) 54–64, https://doi.org/10.1016/j.compositesa.2016.12.022.

[7] H.-C. Tseng, R.-Y. Chang, C.-H. Hsu, Improved fiber orientation predictions for injection molded fiber composites, Compos. Part A 99 (2017) 65–75, https://doi.org/10.1016/j.compositesa.2017.04.004.

[8] M.J. Cieslinski, P. Wapperom, D.G. Baird, Fiber orientation evolution in simple shear flow from a repeatable initial fiber orientation, J. Non-Newtonian Fluid Mech. 237 (2016) 65–75, https://doi.org/10.1016/j.jnnfm.2016.10.003.

[9] R.P. Hegler, G. Mennig, Phase separation effects in processing of glass-bead- and glass-fiber-filled thermoplastics by injection molding, Polym. Eng. Sci. 25 (1985) 395–405, https://doi.org/10.1002/pen.760250704.

[10] J.G. Kovács, Shrinkage alteration induced by segregation of glass beads in injection molded PA6: experimental analysis and modeling, Polym. Eng. Sci. 51 (2011) 2517–2525, https://doi.org/10.1002/pen.22025.

[11] J.L. Colón Quintana, T. Heckner, A. Chrupala, J. Pollock, S. Goris, T. Osswald, Experimental study of particle migration in polymer processing, Polym. Compos. (2018) 13, https://doi.org/10.1002/pc.25018.

[12] A. Kumar, M.D. Graham, Mechanism of margination in confined flows of blood and other multicomponent suspensions, Phys. Rev. Lett. 109 (2012)https://doi.org/10.1103/PhysRevLett.109.108102.

[13] M.S. Ingber, A.L. Graham, L.A. Mondy, Z. Fang, An improved constitutive model for concentrated suspensions accounting for shear-induced particle migration rate dependence on particle radius, Int. J. Multiphase Flow 35 (2009) 270–276, https://doi.org/10.1016/j.ijmultiphaseflow.2008.11.003.

[14] P.R. Nott, J.F. Brady, Pressure-driven flow of suspensions: simulation and theory, J. Fluid Mech. 275 (1994) 157, https://doi.org/10.1017/s0022112094002326.

[15] M.V. Wang, A. Fatahul, V.H. Vu, The study of optimal molding of a LED lens with grey relational analysis and molding simulation, Period. Polytech. Mech. Eng. 63 (2019) 278–294, https://doi.org/10.3311/PPme.13337.

[16] G.-Y. Liu, W.-J. Xu, N. Govender, D.N. Wilke, A cohesive fracture model for discrete element method based on polyhedral blocks, Powder Technol. 359 (2019) 190–204, https://doi.org/10.1016/j.powtec.2019.09.068.

[17] M. Pasha, N.L. Hekiem, X. Jia, M. Ghadiri, Prediction of flowability of cohesive powder mixtures at high strain rate conditions by discrete element method, Powder Technol. 372 (2020) 59–67, https://doi.org/10.1016/j.powtec.2020.05.110.

[18] E. Badakhshan, A. Noorzad, A. Bouazza, Y.F. Dafalias, S. Zameni, L. King, Load recovery mechanism of arching within piled embankments using discrete element method and small scale tests, Powder Technol. 359 (2020) 59–75, https://doi.org/10.1016/j.powtec.2019.10.025.

[19] H. Yu, W. Cheng, L. Wu, H. Wang, Y. Xie, Mechanisms of dust diffuse pollution under forced-exhaust ventilation in fully-mechanized excavation faces by CFD-DEM, Powder Technol. 317 (2017) 31–47, https://doi.org/10.1016/j.powtec.2017.04.045.

[20] M. Mohseni, B. Peters, M. Baniasadi, Conversion analysis of a cylindrical biomass particle with a DEM-CFD coupling approach, Case Stud. Therm. Eng. 10 (2017) 343–356, https://doi.org/10.1016/j.csite.2017.08.004.

[21] G. Liu, F. Yu, S. Wang, P. Liao, W. Zhang, B. Han, H. Lu, Investigation of interstitial fluid effect on the hydrodynamics of granular in liquid-solid fluidized beds with CFD-DEM, Powder Technol. 322 (2017) 353–368, https://doi.org/10.1016/j.powtec.2017.08.048.

[22] Z. Hou, X. Tian, Z. Zheng, J. Zhang, L. Zhe, D. Li, A.V. Malakhov, A.N. Polilov, A constitutive model for 3D printed continuous fiber reinforced composite structures with variable fiber content, Compos. Part B 189 (2020)https://doi.org/10.1016/j.compositesb.2020.107893.

[23] P. Wang, B. Zou, S. Ding, C. Huang, Z. Shi, Y. Ma, P. Yao, Preparation of short CF/GF reinforced PEEK composite filaments and their comprehensive properties evaluation for FDM-3D printing, Compos. Part B 191 (2020)https://doi.org/10.1016/j.compositesb.2020.108175.

[24] K. Liu, W. Li, S. Chen, W. Wen, L. Lu, M. Liu, C. Zhou, B. Luo, The design, fabrication and evaluation of 3D printed gHNTs/gMgO whiskers/PLLA composite scaffold with honeycomb microstructure for bone tissue engineering, Compos. Part B 192 (2020)https://doi.org/10.1016/j.compositesb.2020.108001.

[25] R. Boros, P.K. Rajamani, J.G. Kovács, Combination of 3D printing and injection molding: overmolding and overprinting, Express Polym Lett 13 (2019) 889–897, https://doi.org/10.3144/expresspolymlett.2019.77.

[26] H. Wu, G. Zhao, J. Wang, G. Wang, M. Zhang, A kind of special weld lines with high specific strength and elongation obtained by core-back chemical foam injection molding, Express Polym Lett 13 (2019) 1041–1056, https://doi.org/10.3144/expresspolymlett.2019.91.

[27] Y. Ismail, D. Yang, J. Ye, Discrete element method for generating random fibre distributions in micromechanical models of fibre reinforced composite laminates, Compos. Part B 90 (2016) 485–492, https://doi.org/10.1016/j.compositesb.2016.01.037.

[28] B.D. Le, F. Dau, J.L. Charles, I. Iordanoff, Modeling damages and cracks growth in composite with a 3D discrete element method, Compos. Part B 91 (2016) 615–630, https://doi.org/10.1016/j.compositesb.2016.01.021.

[29] L. Wan, D. Yang, Y. Ismail, Y. Sheng, 3D particle models for composite laminates with anisotropic elasticity, Compos. Part B 149 (2018) 110–121, https://doi.org/10.1016/j.compositesb.2018.05.022.

[30] M. Yu, B. Yang, Y. Chi, J. Xie, J. Ye, Experimental study and DEM modelling of bolted composite lap joints subjected to tension, Compos. Part B 190 (2020)https://doi.org/10.1016/j.compositesb.2020.107951.

[31] C. O'Sullivan, J.D. Bray, Selecting a suitable time step for discrete element simulations that use the central difference time integration scheme, Eng. Comput. 21 (2004) 278–303, https://doi.org/10.1108/02644400410519794.